ECS Journal of Solid State Science and Technology, **1** (3) Q57-Q61 (2012)
2162-8769/2012/1(3)/Q57/5/$28.00 © The Electrochemical Society

Study of Electric Faucet Structure by Embedding Co Nanocrystals in a FeO_x-Based Memristor

Yao-Feng Chang,[a] Yu-Ting Tsai,[b,*] Yong-En Syu,[c] and Ting-Chang Chang[c,d,z]

[a]*Department of Electrical and Computer Engineering, The University of Texas at Austin, Texas 78758, USA*
[b]*Department of Electronics Engineering and Institute of Electronics, National Chiao Tung University, Hsinchu 300, Taiwan*
[c]*Department of Physics, National Sun Yat-Set University, Kaohsiung 804, Taiwan*
[d]*Advanced Optoelectronics Technology Center, National Cheng Kung University, Tainan 701, Taiwan*

The electric faucet concept was realized and demonstrated by embedding cobalt nanocrystals in a $TiN/SiO_2/FeO_x/FePt$ structure. The thermal annealing induced cobalt nanocrystals in silicon oxide would shrink both the operation voltage and variation as well as improves the electric faucet stability. The thickness effect and area size effect would be discussed, which indicated the optimized design and possible resistive switching mechanism for the FeO_x-based memristor. The improvement of resistive switching stabilities and switching power characteristics show that the embedded nanocrystals in the insulating layer would localize the electric faucet formation and rupture at interface region. Importantly, a proposed mathematical model to describe the compliance current effect shows that the electric faucet was grown in two dimensions. These electrical results not only provide a possible physical picture to image the dynamic characteristics of the electric faucet's growth, but also introduce a possible mathematical method to quantify the electric faucet properties.
© 2012 The Electrochemical Society. [DOI: 10.1149/2.020203jss] All rights reserved.

Manuscript submitted March 1, 2012; revised manuscript received April 16, 2012. Published August 14, 2012.

Recently, resistance random access memory (RRAM), phase change memory and discrete nanocrystal memory attract extensive interests for being promising candidates of next generation nonvolatile memory devices due to their excellent advantages of high cell density array, fast operation speed, low power consumption, cheap manufacturing cost, and robust reliability.[1–3] For RRAM, operation variation, device stability and operation current are the most important issues for its commercialized requirements. Several kinds of methods have been proposed, such as doping and implanting metal atoms into the resistive switching materials,[4–6] or embedded nanocrystals in the matrix,[7,8] but still, the electrical stability and operation variation are still an unsolved issues for practical applications. Recently, Inoue et al. have reported a basic physical concept, an electric faucet model, to describe the resistive switching phenomena.[9] In concept, the resistive switching mechanism is resulted from opening or closing the "electric faucet" at the interface region, transferred between low-resistance state (LRS) and high-resistance state (HRS). Therefore, the electrical switching characteristics should be much stabilized because of the localized switching faucet. However, no exact structures could actually realize this physical concept.[10,11] Therefore, in this paper, the electric faucet model is faithfully realized in FeO_x-based memristors by embedded cobalt nanocrystals in a $TiN/SiO_2/FeO_x/FePt$ structure. A thin FeO_x-transition layer, at the interface between SiO_x and Fe-containing electrode, can be as an electric faucet to control the resistance states, and its thickness can be further reduced below 5 nm. Moreover, the resistive switching characteristics can be markedly improved due to the inhomogeneous electric field facilitated by embedding nanocrystals in the SiO_2. The electrical statistics results and several physical structures cannot only help in constructing a possible physical picture for the switching mechanism, but also further quantify the dynamic characteristics of the electric faucet's growth behavior in FeO_x-based memristors.

Experimental

The process realized the electric faucet structure in the FeO_x-based memristor was as following. After thermal oxidation of *p*-type (100) silicon wafers, a 50-nm-thick $Fe_{0.73}Pt_{0.27}$ layer, determined by inductively coupled plasma mass spectroscopy, was also cosputtered with Fe and Pt targets as a bottom electrode. A 25-nm-thick SiO_2 layer was deposited on the bottom electrode by a plasma enhanced chemical vapor deposition (PEVCD) system with substrate temperature of 300°C and a working pressure of (TEOS(50sccm)+O_2(300sccm)) gases at 500 mTorr as well as for a 11-nm-thick SiO_2 layer device. The Co thin film was sputtered on the SiO_x film in the Ar ambient for 30 sec at a nominal deposition rate of 0.1 nm/s, and then, the devices cap the same thickness of SiO_x layer by previous condition for each device (denoted as "SiO_x-50 nm sample" and "SiO_x-22 nm sample", respectively). The top electrode, 50-nm-thick TiN, was sputtered and patterned in a square area with side length of 100 μm on the SiO_2 film for most of the devices except of area size effect. Finally, rapid thermal annealing (RTA) treatments at 700°C for different intervals of 30 sec (denoted as "RTA-30 sec sample"), and 60 sec (denoted as "RTA-60 sec sample") were performed in Argon ambient. For comparison, a control sample without the annealing treatment (denoted as "as-deposited sample") was also prepared under the same process. A Keithley 4200 semiconductor characterization system was used to measure the current-voltage (*I-V*) characteristics of the fabricated devices. In addition, transmission electron microscopy (TEM) and X-ray photoelectron spectroscopy (XPS) were carried out using a Philips Tecnai-20 System and the Microlab 350 with a monochromatized Al Kα X-ray source (1486.6 eV; 300 W), respectively. In order to gain more insight during the resistance switching process, electric parameters of critical switching conditions were extracted for all the samples. The definition of the "Set Current/Reset Current (I_{set})/(I_{reset})" and "Set Voltage/Reset Voltage (V_{set})/(V_{reset})" are the values of the current and voltage detected at the beginning of the resistance switching from a HRS/LRS to a LRS/HRS, respectively. The definition of the "LRS Current"/"HRS Current" is the value of the current measured in the LRS/HRS at a voltage bias of 0.5 V.

Results and Discussion

Fig. 1 shows the 50 cycles of switching *I-V* characteristics for the as-deposited SiO_x-50 nm sample. The driving voltage was biased on the bottom electrode while the top electrode was ground and the compliance current was limited to 5 mA to prevent the hard breakdown during sweeping voltage. After the electroforming process, bipolar switching is observed on sweeping the voltage from 0 V to positive values and the current begins to decrease gradually at a reset voltage (V_{reset}) and finally reaches a high resistance state (HRS). On the other hand, the current increases suddenly at a set voltage (V_{set}) and returns to a low resistance state (LRS) while sweeping the voltage to negative values. In addition, besides an increase in operation voltages (V_{set} and V_{reset}), the variances of V_{set} (ΔV_{set}) and V_{reset} (ΔV_{reset}) were also degraded as the thickness of SiO_x layer increased. Moreover, by using TEM analysis, as shown the inset in Fig. 1, the device size (reduced

*Electrochemical Society Student Member.
zE-mail:tcchang@mail.phys.nsysu.edu.tw

Downloaded on 2014-04-28 to IP 140.113.38.11 address. Redistribution subject to ECS terms of use (see ecsdl.org/site/terms_use) unless CC License in place (see abstract).

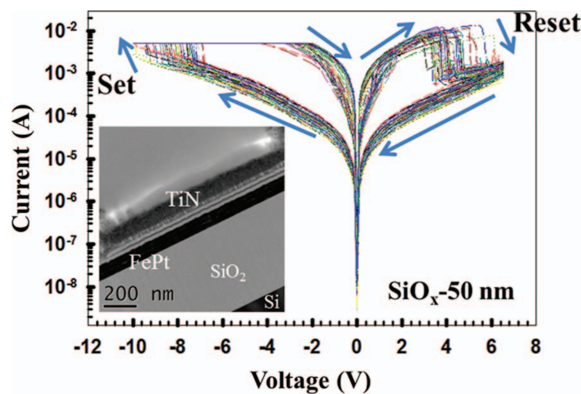

Figure 1. 50 cycles of bipolar switching behaviors of as-deposited SiO_x-50 nm sample and with compliance current 5 mA. The arrows indicate voltage sweeping directions. The inset of Fig. 1 shows the cross-sectional TEM image of the small size (1.5 μm × 5 μm) $TiN/SiO_2/FeO_x/FePt$ structure with inserted a cobalt thin film.

to 1.5 μm × 5 μm), the thickness of each layer, and the inserted Co thin film can be confirmed. Also, it was further observed that there was a thin gray layer of about (or below) 5 nm in thickness between SiO_2 and FePt layer, associated with the FeO_x transition region by energy dispersive X-ray (EDX) analysis. In our previous reports, a thin FeO_x-transition layer at the silicon oxide/Fe-containing electrode interface could be regarded as an electric faucet, which means that the device's resistance states are dominated by the electric-induced chemical redox reaction between Fe_2O_3 (HRS) and F_3O_4 (LRS).[12,13] Of note, as comparison the thickness effect for the electrical characteristics, a reduction of the SiO_x thickness could result in increasing the switching power efficiency, in other words, the switching power could be more effectively applied to the resistive switching layer, a thin FeO_x-transition layer, and further reduce the operation voltage and its variation.[14] Also, the HRS current for the as-deposited SiO_x-22 nm sample is higher than the as-deposited SiO_x-50 nm sample as well as for the thermal treatment samples at same operation conditions (discuss later). The possible reason is that the thinner device provides less resistance and oxygen supplying to the resistive switching layer, which results in a small parasitical resistance (high leaky device) and less Fe_2O_3 transformation.

The devices were further performed thermal treatment for both of structures, and the *I-V* electrical switching characteristics could be markedly improved, as shown in Fig. 2. Figure 2 shows the *I-V* characteristics of the RTA-30 sec of SiO_x-50 nm and SiO_x-22 nm samples for 50 cycles of switching, respectively. The results suggested that the thermal treatment would reduce the operation voltages as well as electrical variation as comparison to the as-deposited samples. we suggest that the improved crystallinity of the FeO_x film, i.e. been already existed crystalline phases of Fe_2O_3 structure in the annealed sample, could cause the ease of such iron oxide phase transformation between Fe_3O_4 and Fe_2O_3 so as to reduce the operation voltages as well as their variations.[15] Moreover, besides of severe Fe ions diffusion effect induced ΔV_{set} and ΔV_{reset} decreased, the thermal annealing effect for inserted Co thin film in FeO_x-based memristor could further improved its electrical stability. Of note, the RTA-60 sec of SiO_x-50 nm sample has the largest LRS/HRS current ratio because of the lower HRS current compared to the RTA-60 sec of SiO_x-22 nm sample, which may attribute from the trade-off between the diffusion effect of Fe atoms and the thickness of FeO_x-transition layer. For comprehensive comparison with the SiO_x thickness effect and thermal treatment effect, Table I shows the tendency of the mean value and its corresponding coefficient of variation, defined as the percentage of standard deviation/mean value, of Set (Reset) electrical parameters and LRS (HRS) current.

The thermal treatment effect was examined in detail by using TEM and XPS analyzes for RTA-60 sec of SiO_x-50 nm sample (RTA-30 sec are similar to the RTA-60 sec sample, therefore, its data are not shown here), as shown in Fig. 3a and 3b. In Fig. 3a, the cross-sectional TEM image shows that an approximate 50 nm thick SiO_x layer embedded with Co nanocrystals. The aerial density and mean size of the Co nanocrystals are measured to be $2.13 \times 10^{12}/cm^2$ and 4-6 nm, respectively. The high resolution TEM image in the inset of Fig. 3a shows a lattice image of nanocrystals, indicating that the inserting Co thin film was crystallized after 700°C annealing treatment. To further investigate the chemical composition of the Co nanocrystals, XPS analysis was performed for the as-deposited and RTA-60 sec of SiO_x-50 nm samples. Figure 3b shows the Co 2p2/3 core-level photoemission spectrum, which consists of two main peaks (780.9 eV and 777.8 eV) with small satellite peaks for as-deposited sample,

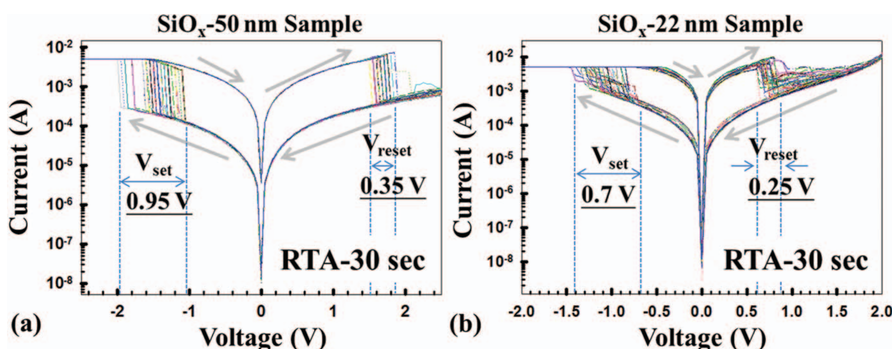

Figure 2. 50-cycle bipolar switching behaviors of the RTA-30 sec at 700°C thermal-treated (a) SiO_x-50 nm and (b) SiO_x-22 nm samples, respectively. The arrows indicate the variations of set and reset voltage value.

Table I. Comparison of the mean value and coefficient of variation of set & reset voltage, set & reset current and HRS & LRS current of the SiO_x-50 nm sample and SiO_x-22 nm sample between the as-deposited and RTA-60 sec annealed conditions.

SiO_x-22nm	Vset (V) (%)	Iset (mA) (%)	Vreset (V) (%)	Ireset (mA) (%)	HRS (mA) (%)	LRS (mA) (%)
As-dep.	4.50 (9.07)	2.17 (43.09)	2.55 (13.69)	8.30 (18.48)	5.60E-02 (40.51)	1.26 (31.76)
RTA-60s	0.70 (8.38)	0.33 (16.89)	0.86 (10.03)	5.81 (13.91)	0.23 (19.12)	3.45 (6.15)
SiO_x-50 nm	Vset (V) (%)	Iset (mA) (%)	Vreset (V) (%)	Ireset (mA) (%)	HRS (mA) (%)	LRS (mA) (%)
As-dep.	8.10 (10.23)	1.98 (33.45)	3.79 (20.15)	8.74 (23.48)	1.67E-02 (25.20)	0.54 (82.74)
RTA-60s	0.91 (13.64)	0.29 (26.33)	0.77 (4.90)	6.42 (7.18)	0.11 (2.61)	4.02 (3.64)

Downloaded on 2014-04-28 to IP 140.113.38.11 address. Redistribution subject to ECS terms of use (see ecsdl.org/site/terms_use) unless CC License in place (see abstract).

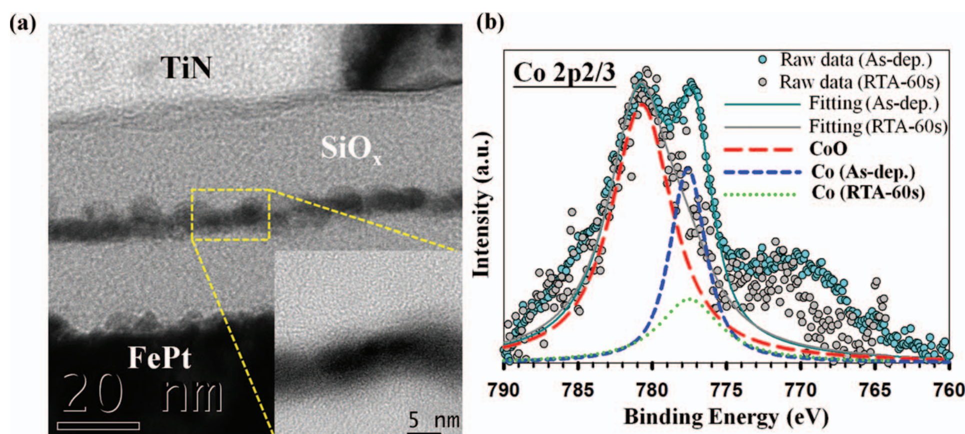

Figure 3. (a) The cross-sectional TEM images of RTA-60 sec at 700°C thermal-treated SiO_x-50 nm samples, (b) XPS Co 2p2/3 spectra between the as-deposited and RTA-60 sec SiO_x-50 nm samples.

and one main peak (780.9 eV) with small satellite peaks for RTA-60 sec sample, respectively. According to the binding energy values estimated in the literature, the binding energy values of the metallic cobalt (Co-Co) and Co oxide (Co-O) are at 777.8 eV and 780.9 eV, respectively.[16] In Fig. 3b, it could be observed that the major chemical composition in Co nanocrystals is Co oxide due to processing enough thermal energy during the post-thermal treatment and sufficiently oxygen-supplied environment in the SiO_x layer. Not only these nanocrystals in the middle of SiO_x matrix would enhance the localized vertical electric field,[7] but also the high density of traps and defects existing around the oxidized Co/CoO_x core/shell nanocrystals[3] would provide several preferred paths for the electric channel formation. Therefore, after the electroforming process, the electric channel would be formed in the SiO_x matrix and further connect to the electric faucet at the interface region, a thin FeO_x-transition layer. Of note, an electroforming process was required for all devices before repeating switching measurements. The current-controlled electroforming process was performed to activate the memristors due to the high yield consideration and precisely control the filaments or electric channel formation.[17,18] After a 700°C annealing for 60 sec, the electroforming electric field of the as-deposited sample was reduced from 3.81 MV/cm to 3.26 MV/cm. It could be associated with that the Co nanocrystals enhanced the localized electric field during the electroforming process, and then further reduced the operation voltages and its electrical variation during repeating switching measurements.

Although the resistive switching mechanism and characteristics of FeO_x-based memristors have been investigated, further understanding the switching mechanism by different area size effect has not yet been done.[12,13] In Fig. 4a, different area size dependence of resistance values in HRS and LRS was investigated by RTA-60 sec of SiO_x-50 nm sample. Interestingly, the resistance in HRS depends more obviously and strongly on the electrode area size, suggesting that the HRS current wholly flows through the entire electrode area and associating with the homogeneous interface-type resistive switching phenomenon. On the other hand, the resistance in LRS shows a slight dependence on the area size, suggesting that the LRS current is combined with both an entire area phenomenon and a localized phenomenon, associating with the minority of interface-type resistive switching phenomenon and the majority of inhomogeneous filament-type resistive switching phenomenon. Therefore, in the embedded Co nanocrystals of $TiN/SiO_2/FeO_x$/Fe-containing structure, the physical concept of the electric faucet model can be faithfully realized, and the resistive switch is dominated by a thin FeO_x-transition layer at the interface, transited between homogeneous (HRS) and inhomogeneous (LRS) states.

Fig. 4b shows the extracting set power density and reset power as function of different area size for RTA-60 sec of SiO_x-50 nm sample. The definition of the "set power/reset power" is the values of the current and voltage detected at the beginning of the resistance switching from a HRS/LRS to a LRS/HRS, especially for the definition of the set power density, is set power divided by the corresponding area size. In Fig. 4b, both of the set power density, related to the homogeneous interface-type resistive switching, and reset power, related to the inhomogeneous filament-type resistive switching, is independent with electrode area. Based on the recently studies, the set power and reset power at the initial current change point can be regarded as the beginning of chemical reduction reaction, which means that the resistance state is beginning to transfer from HRS (LRS) to LRS (HRS).[13,14] Therefore, the same transformation energy of redox reaction from Fe_2O_3 phase to Fe_3O_4 phase in the FeO_x-transition layer can be predicted for all the samples, and the applied set power should be approximate constant when we exclude the power consumption within the SiO_x layer.

Based on the above analysis, the possible scenario for the resistive switching process is described as following: During the electroforming process, the electric channel would be formed along the preferred paths or enhanced electric field location; meanwhile, the electric faucet at the interface region would be opened in the set process due to the electric-induced chemical redox reaction from Fe_2O_3 (HRS) to Fe_3O_4 (LRS). The set power would pass through the entire area due to the HRS is associated with the homogeneous interface-type resistive switching phenomenon. Therefore, the set power density would be independent with the active size. On the other hand, for

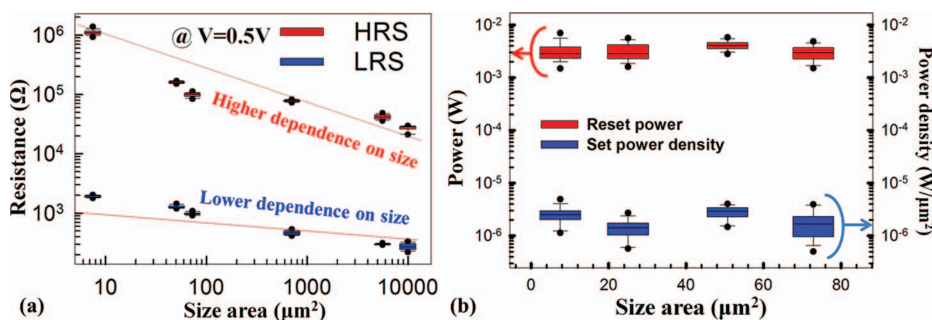

Figure 4. Electrode area dependence of (a) resistance values in high and low resistance states and (b) set power density and reset power for the RTA-60 sec at 700°C thermal-treated SiO_x-50 nm samples.

Downloaded on 2014-04-28 to IP 140.113.38.11 address. Redistribution subject to ECS terms of use (see ecsdl.org/site/terms_use) unless CC License in place (see abstract).

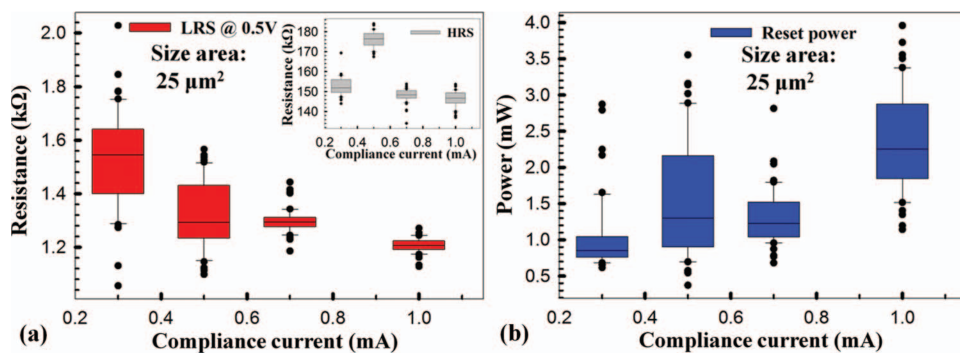

Figure 5. (a) Statistics plots of LRS and HRS resistance (inset) as a function of compliance current. (b) Statistics plots of reset power as a function of compliance current. Device area is 25 μm^2.

the reset process, the electric faucet at the interface region would be "closed" due to the inverse electric-induced chemical redox reaction from Fe_3O_4 (LRS) to Fe_2O_3 (HRS). The major LRS current would pass along the electric channel (filament-type resistive switching phenomenon) then contribute the current-induced Joule heating energy to the localized electric faucet region. Therefore, the reset power would be independent with the active electrode area.

According to our previous discussion, the electric faucet structure and its characteristics have been realized and studied in FeO_x-based memristors. In this section, we aggressively analyzed the electric faucet growth behavior by controlling compliance current limitation. In the beginning, clarify the conduction mechanism of the insulating SiO_x layer in FeO_x-based memristors is important. Several structures, such as different top electrodes (TiN, Al and W-probe)/SiO_2/different bottom electrodes (Pt, Fe and FePt), and their corresponding electrical characteristics are examined (not shown here). The results show that the SiO_x layer, deposited by TEOS source and PECVD method, has a good insulator property (the electrical breakdown field is about 5 MV/cm). After the electroforming process, its resistance is about 10 Ω at 0.5 V reading in the Al/SiO_2/Pt structure due to the generated Si interstitials or defects percolate to form low resistance paths.[19] On the other hand, the resistance of the FeO_x-based memristors is dominated by a thin FeO_x-transition layer which is approximated as 0.3 kΩ at 0.5 V reading in LRS (ignore the resistance of the SiO_x layer) from Table I. The relationship can be described as following:

$$R_{SiO_x} < R_{FeO_x} \quad [1]$$

Second, the compliance current effect at fixed stopped voltage for the resistance of LRS and HRS (inset in Fig. 5a) and reset power is studied by analyzing the statistic electrical results in 50 times cycling, as shown in Fig. 5a and 5b, respectively. In Fig. 5a, the mean value of the LRS resistance as well as its corresponding variation decreases with the increase of compliance current, but, however, the HRS resistance is nearly constant and just has small variation values compared to the LRS resistance. These electrical results suggest that the electric faucet may suffer a different level of Joule heating energy or contributed hopping charges in the chemical reaction process, and result in adjustable LRS from approximately fixed HRS.[14,20] Furthermore, according to the Ohmic law, the relationship between the resistance of FeO_x-transition layer ($R_{FeO_x}|_{average}$, ignore the resistance of the SiO_x layer in the FeO_x-based memristors due to its low resistance after the electroforming process) and its corresponding electric faucet cross-sectional area ($A_{average}$) can be described as following:

$$\text{Ohmic law}: R_{FeO_x}|_{average} = \rho_{FeO_x}\frac{d_{transition}}{A_{average}} \quad [2]$$

ρ_{FeO_x} is the resistivity of the FeO_x-transition layer and $d_{transition}$ represents the FeO_x-transition layer thickness. This formula implies that the electric faucet resistance can be controlled by adjusting two factors in compliance current effect: 1 the average cross-sectional area of electric faucet and 2 the resistivity of the FeO_x-transition layer. That is to say, in compliance current effect, the resistance variation would increase (decrease) because of smaller (larger) cross-sectional area of electric faucet. Based on the above described physical picture, the reset power trend could further support the same idea, which means that the smaller reset power would be required to recover the oxygen vacancies in the FeO_x-transition layer and then change its phase or area for the smaller electric faucet. Of note, the reset power could not decrease effectively with compliance current due to the existed parasitical capacitance for the external clamping controller.[21]

The statistic electrical results in compliance current effect were examined in detail by using a mathematical method to quantify the electrical faucet growth behavior. First, several definitions should be mentioned to make more insight in the proposed mathematical model: the definition of the "average cross-sectional area of electric faucet (μ)" is the average value of the whole LRS reading current in 50 cycles.

$$\text{Electric faucet average cross-sectional area}: \mu = \frac{\sum_{i=1}^{n} X_i}{n} \quad [3]$$

Also, the electric faucet deviation and its variation are defined by the statistic standard deviation (σ) and coefficient of variation (COV) of whole 50 cycles of LRS reading current, respectively.

$$\text{Electric faucet deviation}: \sigma = \sqrt{\frac{\sum_{i=1}^{n}(x_i - \mu)^2}{n}} \quad [4]$$

$$\text{Electric faucet variation}: COV = \frac{\sigma}{\mu} \quad [5]$$

In Fig. 6, it represents the relationship of average electric faucet cross-sectional area and its corresponding variation as function of the compliance current limitation by using these mathematical analyzes.

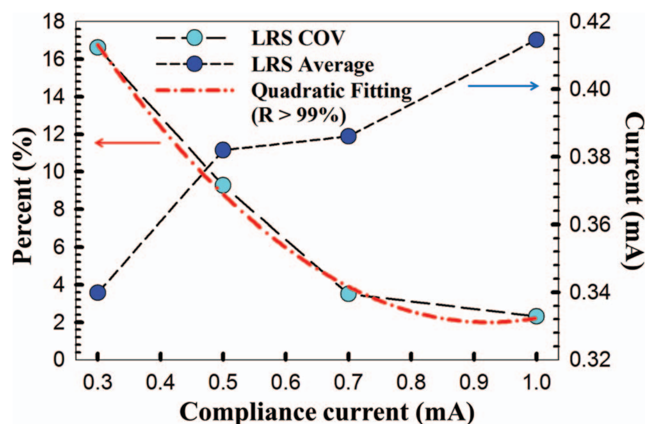

Figure 6. (a) The relation between LRS average and coefficient of variation as function of compliance current. The red dash fitting line shows a quadratic function between 0.3 mA to 1.0 mA.

Downloaded on 2014-04-28 to IP 140.113.38.11 address. Redistribution subject to ECS terms of use (see ecsdl.org/site/terms_use) unless CC License in place (see abstract).

The results clearly indicate the electric faucet growth behavior: the larger compliance current limitation would results in larger cross-sectional area of electric faucet and then decrease its variation. Importantly, the quadratic fitting result for the electric faucet variation implies that the electric faucet is growth in two-dimension. Although Russo et al. have performed the similar simulation results in NiO_x system,[22] however, the mathematical statistics analysis by using the experimental data is the first time. The possible explanation for the two-dimension growth behavior is that not only the electric faucet radius would be changed by the compliance current level, but also the chemical composition in the electric faucet would be adjusted.[13] Further investigation for the statistics of the electrical switching parameters is still undergoing.

Conclusions

In conclusion, the electric faucet structure by embedding Co nanocrystals in the FeO_x-based memristors was successfully demonstrated. The thickness effect and area size effect indicated the optimized design and physical concept of the resistive switching mechanism, respectively. Moreover, a mathematical statistics method was proposed, which further described the electric faucet growth behavior in compliance current effect. The electric faucet concept and structure cannot only improve the basic electrical switching characteristics, but also possibly reduce the switching energy due to the localized nanoscale behavior for the future resistive switching memory requirements.

Acknowledgments

This work was performed at National Science Council Core Facilities Laboratory for Nano-Science and Nano-Technology in Kaohsiung-Pingtung area and was supported by the National Science Council of the Republic of China under Contract Nos. NSC 100-2120-M-110-003.

References

1. B. Govoreanu, G. S. Kar, Y.-Y. Chen, V. Paraschiv, S. Kubicek, A. Fantini, I. P. Radu, L. Goux, S. Clima, R. Degraeve, N. Jossart, O. Richard, T. Vandeweyer, K. Seo, P. Hendrickx, G. Pourtois, H. Bender, L. Altimime, D. J. Wouters, J. A. Kittl, and M. Jurczak, *Tech. Dig. - Int. Electron Devices Meet*, 729 (2011).
2. M. J. Kang, T. J. Park, Y. W. Kwon, D. H. Ahn, Y. S. Kang, H. Jeong, S. J. Ahn, Y. J. Song, B. C. Kim, S. W. Nam, H. K. Kang, G. T. Jeong, and C. H. Chung, *Tech. Dig. - Int. Electron Devices Meet*, 39 (2011).
3. T. C. Chang, F. Y. Jian, S. C. Chen, and Yu-Ting Tsai, *Mater. Today*, **14**, P526 (2011).
4. Q. Liu, W. H. Guan, S. B. Long, M. Liu, S. Zhang, Q. Wang, and J. N. Chen, *J. Appl. Phys.*, **104**, 114514 (2008).
5. Q. Liu, W. H. Guan, S. B. Long, R. Jia, M. Liua, and J. N. Chen, *Appl. Phys. Lett.*, **92**, 012117 (2008).
6. H. W. Zhang, B. Gao, B. Sun, G. P. Chen, L. Zeng, L. F. Liu, X. Y. Liu, J. Lu, R. Q. Han, J. F. Kang, and B. Yu, *Appl. Phys. Lett.*, **96**, 123502 (2010).
7. Y. T. Tsai, T. C. Chang, C. C. Lin, S. C. Chen, C. W. Chen, S. M. Sze, F. S. Yeh, and T. Y. Tseng, *Electrochem. Solid-State Lett.*, **14**, H135 (2011).
8. L. Chen, H. Y. Gou, Q. Q. Sun, P. Zhou, H. L. Lu, P. F. Wang, S. J. Ding, and D. W. Zhang, *IEEE Electron Device Lett.*, **32**, 794 (2011).
9. I. H. Inoue, S. Yasuda, H. Akinaga, and H. Takagi, *Physical Review B*, **77**, 035105 (2008).
10. G. S. Park, X. S. Li, D. C. Kim, R. J. Jung, and M. J. Lee, *Appl. Phys. Lett.*, **91**, 222103 (2007).
11. R. Soni, P. Meuffels, H. Kohlstedt, C. Kügeler, and R. Waser, *Appl. Phys. Lett.*, **94**, 123503 (2009).
12. L. W. Feng, C. Y. Chang, Y. F. Chang, W. R. Chen, S. Y. Wang, P. W. Chiang, and T. C. Chang, *Appl. Phys. Lett.*, **96**, 052111 (2010).
13. Y. F. Chang, T. C. Chang, and C. Y. Chang, *J. Appl. Phys.*, **110**, 053703 (2011).
14. C. Rohde, B. J. Choi, D. S. Jeong, S. Choi, J. S. Zhao, and C. S. Hwang, *Appl. Phys. Lett.*, **86**, 262907 (2005).
15. L. W. Feng, C. Y. Chang, Y. F. Chang, T. C. Chang, S. Y. Wang, S. C. Chen, C. C. Lin, S. C. Chen, and P. W. Chiang, *Appl. Phys. Lett.*, **96**, 222108 (2010).
16. M. Oku and K. Hirokawa, *J. Electron Spectrosc. Relat. Phenom.*, **8**, 475 (1976).
17. U. Russo, C. Cagli, S. Spiga, E. Cianci, and D. Ielmini, *IEEE Electron Device Lett.*, **30**, 817 (2009).
18. W. T. Lian, H. B. Lv, Q. Liu, S. B. Long, W. Wang, Y. Wang, Y. T. Li, S. Zhang, Y. H. Dai, J. N. Chen, and M. Liu, *IEEE Electron Device Lett.*, **32**, 1035 (2011).
19. R. Degraeve, G. Groeseneken, R. Bellens, M. Depas, and H. E. Maes, *Tech. Dig. - Int. Electron Devices Meet*, 863 (1995).
20. S. Yu and H. S. Philip Wong, *Tech. Dig. - Int. Electron Devices Meet*, 520 (2010).
21. K. Kinoshita, K. Tsunoda, Y. Sato, H. Noshiro, S. Yagaki, M. Aoki, and Y. Sugiyama, *Appl. Phys. Lett.*, **93**, 033506 (2008).
22. U. Russo, D. Ielmini, C. Cagli, and A. L. Lacaita, *IEEE. Trans. Electron Devices*, **56**, 193 (2009).

Downloaded on 2014-04-28 to IP 140.113.38.11 address. Redistribution subject to ECS terms of use (see ecsdl.org/site/terms_use) unless CC License in place (see abstract).